Ivanov, P., Ho, Y-L. D., Snoswell, D. R. E., Elsner, N. H., Vincent, B., Bower, C., ... Cryan, M. J. (2010). Lattice constant tuning and disorder effects in 3D colloidal photonic crystals. IEEE Journal of Display Technology, 6(1), 14 - 21. 10.1109/JDT.2009.2030347

Lattice Constant Tuning and Disorder Effects in 3D Colloidal Photonic Crystals

Pavel Ivanov, Y.-L. D. Ho, David R. E. Snoswell, Nils Elsner, Brian Vincent, Chris Bower, John G. Rarity, and Martin J. Cryan

***Abstract*—This paper uses the plane-wave expansion and finite-difference time-domain methods to study tunable 3D photonic crystals for use in display applications. The paper calculates particle diameter and refractive index for operation across the visible spectrum and estimates the reflectivity achievable for one to five layers of particles. The effects of disorder in particle position and diameter are then studied and the results show the system to be robust against such effects. Finally, the paper discusses the potential performance of this display technology in terms of reflectivity, color gamut, and contrast ratio.**

***Index Terms*—Displays, electromagnetic fields, FDTD methods, optical reflection.**

I. Introduction

OVER the past few decades, a new optical medium called the photonic crystal (PhC) has emerged. A PhC is a medium where the refractive index of the material has a periodic modulation in one, two, or three directions. PhCs have been successfully used in many modern optical devices, such as lasers and waveguides [1], [2]. Recently, PhCs were applied to new class of displays [3]–[5] allowing tunable color emission from a single pixel. The pixel contains a chamber filled with a PhC made of an ordered array of colloidal particles embedded in a host material. The color of the pixel changes either due to band-pass filtering caused by photonic band-gaps (PBGs) [3], [5] or diffraction [4] effects. In both cases, the change of color of the pixel is achieved by tuning the spacing between spherical colloidal particles.

In our previous work [4] we have demonstrated tuning the color of the pixel due to diffraction effects. Polystyrene particles with a diameter of 945 nm were deposited into a chamber filled with water. A four-electrode system was applied to form a rotating electric field in the chamber which causes particles to be attracted to each other and thus forms hexagonally closed packed "rafts" of particles which act as diffraction gratings. Due to the large size of particles and the lattice constant of the PhC, the expected photonic band gaps at infrared wavelengths were too difficult to observe in these 2D PhCs.

Our own experimental work has since moved to much smaller particles with 200-nm diameter which can form crystals with very rapid electrically tunable structural color with switching times on the order of microseconds [6]. Similar studies on 'polymer opals' [7] and crystals embedded in responsive gels have also emerged that demonstrate tunable stop bands in the visible with particles of this size range [8].

The PhCs that have been used for display applications have a certain level of disorder which arises from polydispersity of particle sizes and particle movements due to Brownian motion and the effect of applied field. It has been reported [9], [10] that the disorder in the PhC affects the stop bands of the PhC, and therefore, disorder effects must be investigated in order to know the limit of the disorder we can allow in the displays. Disorder effects in PhC were studied in [11], but the modeled PhC had many more layers than is anticipated for our colloidal PhC applications. In our system, we show that the effect of additional layers on the PhC is more pronounced for the initial few layers, and therefore helps to determine the limiting design thickness for a PhC suitable for displays. Also, in the previous study [11] only the effect of the deviation of the particle size was considered and the particles were close packed. Here on the other hand, we look independently at both size and positional disorder, matching our experimental conditions where particles are not touching [4], and the lattice spacing can be tuned. Disorder has also been studied for fixed and inverse opal PhC structures [22], [23], however, it is not obvious that these results can be extrapolated on to the low refractive index contrast, non-touching PhC that is considered here.

Thus this paper models the optical properties of PhCs formed with spherical particles, using an in-house 3D finite-difference time-domain (FDTD) code [12] and the plane-wave expansion (PWE) method. In particular this paper focuses on the optimization of particle refractive index and diameter for display applications, and studies the effects of disorder which will occur in any practical realization, including both particle polydispersity and particle position.

The paper is organized as follows. First, we describe the PhC to be studied and analyze its photonic band diagrams using the PWE method. Next, the results of numerical investigations, using the FDTD method, of the PhC reflection coefficient spectra are presented and compared to the results of the PWE method. The effects of the particle size and position variation on the reflection coefficient spectra are then investigated using

Manuscript received March 29, 2009; revised July 03, 2009. Current version published December 09, 2009.

P. Ivanov, Y.-L. D. Ho, J. G. Rarity and M. J. Cryan are with the Department of Electrical and Electronic Engineering, Queen's Building, University of Bristol, Bristol, BS8 1UB, U.K. (e-mail: p.ivanov@bristol.ac.uk; Daniel.Ho@bristol.ac.uk; john.rarity@bristol.ac.uk; m.cryan@bristol.ac.uk).

D. R. E. Snoswell is with the Department of Physical and Theoretical Chemistry, University of Bristol, Cantocks Close, Bristol BS8 1TS, U.K., and also with the Department of Physics, Cavendish Laboratory, University of Cambridge, Cambridge CB3 0HE, U.K. (e-mail: dres2@cam.ac.uk).

N. Elsner and B. Vincent are with the Department of Physical and Theoretical Chemistry, University of Bristol, Cantocks Close, Bristol BS8 1TS, U.K. (e-mail: nils.elsner@bristol.ac.uk; brian.vincent@bristol.ac.uk).

C. Bower is with Nokia Research Centre, University of Cambridge Nanoscience Centre, Cambridge, CB3 0FF, U.K. (e-mail: chris.bower@kodak.com).

Color versions of one or more of the figures in this paper are available online at http://ieeexplore.ieee.org.

Digital Object Identifier 10.1109/JDT.2009.2030347

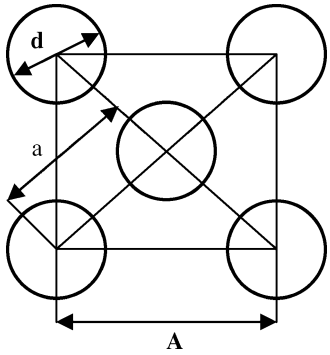

Fig. 1. Schematic 2D representation of the PhC lattice.

the FDTD method. Finally the potential performance of this display technology is investigated using FDTD modeling and estimates of achievable reflectivity and contrast ratio are made. A preliminary study of viewing angle sensitivity study is also included.

II. Photonic Band Diagram of the PhC

In this work a PhC made of spherical particles embedded in water is considered. We assume that spherical particles are ordered in a face-centred cubic (FCC) lattice since shear ordering tends to favour the FCC lattice [21] The refractive index of the particles take two values: 1.6 or 2, and the refractive index of background water is 1.33. A plan view of a unit cell of the structure is shown in Fig. 1. The diameter of particles, d, the FCC lattice constant, A and the centre-to-centre spacing of particles, a are shown in the figure. The spacing varies in the range $a = 200$ to 400 nm and the diameter is fixed at $d = 200$ nm. In order to calculate photonic band diagrams the PWE method from RSOFT [13] was used.

Since in this work we investigate the PBG effect to filter the color of reflected light, the tuneability of the photonic band gap is the key parameter and is considered in this section. The position of the PBG in the spectrum can be tuned by changing the spacing between centres of particles of the FCC lattice which depends on the strength of the applied electric field. Previous work demonstrated that a rapidly rotating electric field produces a time-averaged dipolar attraction in a 2D plane [4]. It should therefore also be possible to time-average dipolar attractions uniformly in three dimensions in a similar method by rapidly varying the direction of the field around a sphere. However, this is very challenging in 3D, requiring three independently controlled time-dependent voltage sources and three pairs of electrodes. One possibility is to use stacked parallel-plate electrodes with electrodes spatially arranged on the corners of a cube.. An alternative geometry we have investigated, uses only 4 electrodes arranged in a tetrahedral geometry, which avoids some of the field distortion effects, but requires a very complex drive system to create a rotating 3D field. In either case one can encounter significant field gradients at electrode edges which cause dielectrophoretic movement of the particles, disrupting crystal formation at high field strengths. Nevertheless, our own unpublished investigations and other research [14] have shown that parallel plate electrodes producing uniform alternating fields can be used to assemble 3D crystals, although dipole attractions may be asymmetric leading to non-FCC structures

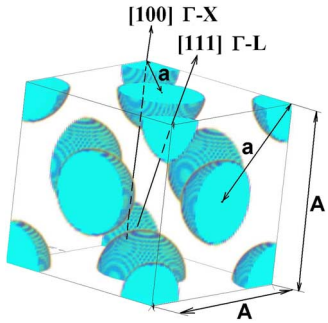

Fig. 2. Diagram showing $\Gamma - \mathrm{L}$ and $\Gamma - \mathrm{X}$ direction in FCC lattice.

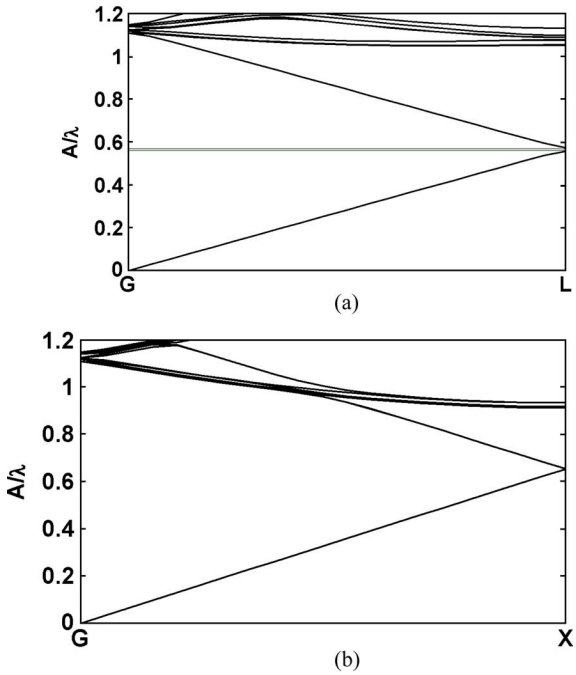

Fig. 3. Photonic band diagram of the PhC with $d = 200$ nm, $a = 200$ nm and $n = 1.6$ (a) $\Gamma - \mathrm{L}$, (b) $\Gamma - \mathrm{X}$. The lattice constant of the FCC lattice $A = a\sqrt{2}$.

[14]. In summary, we are satisfied that 3D PhCs with visible stopbands can be assembled and tuned by induced dipole forces, similar to our previous publication on 2D. The calculations presented in this paper bear direct relevance to the tuneable 3D PhCs we have generated, the details of which will be detailed in a future publication pending a patent application [6].

It is well known that a *complete* PBG cannot be achieved for refractive index differences as low as being studied in this work, however, for display applications band gaps in particular directions may be sufficient. Fig. 2 shows two of the main directions which characterise the FCC lattice, these are known as $\Gamma - \mathrm{L}$ and $\Gamma - \mathrm{X}$.

Fig. 3 shows the photonic band diagrams of the PhC created by colloidal particles with refractive index $n = 1.6$, diameter $d = 200$ nm and distance between centres of particles $a = 200\,\mathrm{nm}\,(d/a = 1)$. Periodic boundary conditions were assumed at all boundaries of the simulation domain. A complete PBG for all directions in the PhC was not found, but a bandgap for the $\Gamma - \mathrm{L}$ direction was found as shown by the gray region in Fig. 3(a). For this reason, this paper concentrates on the $\Gamma - \mathrm{L}$ direction only. It is worth noting that the $\Gamma - \mathrm{L}$ direction is normally

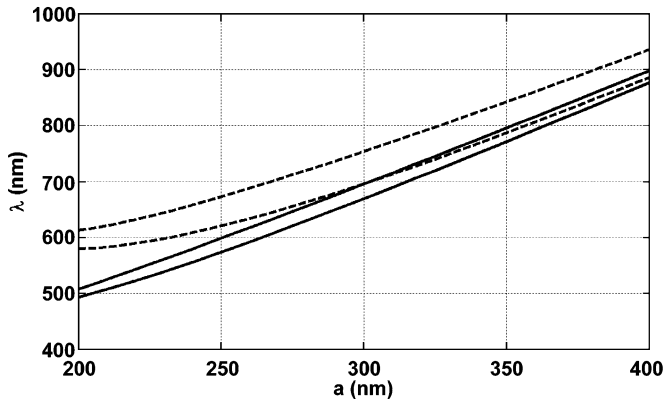

Fig. 4. The position of the edges of the $\Gamma - \mathrm{L}$ band gap in wavelength domain versus the centre-to-centre spacing of the FCC lattice and two values of n, $d = 200$ nm (solid line: $n = 1.6$, dashed line: $n = 2$).

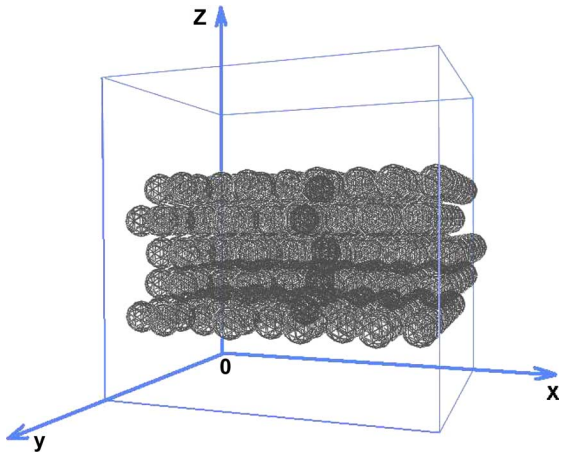

Fig. 5. FDTD model of a FCC lattice showing five layers.

perpendicular to the substrate surface for standard FCC lattices [15].

The size of particles required to give strong reflection at a given wavelength can be computed from the band structure shown in Fig. 3(a). Since the PBG of the PhC in $\Gamma - \mathrm{L}$ direction appears at $A/\lambda = 0.58$, the corresponding centre-to-centre spacing is $A = 232$ nm for light of wavelength $\lambda = 400$ nm. Consequently the diameter of particles in this case is $d = a = 164$ nm.

We are interested in tuning the partial PBG shown in Fig. 3(a) across the visible range of wavelengths from 400 nm to 650 nm by varying the particle-to-particle spacing, a. Thus the results of Fig. 3(a) above have been recalculated for a range of particle spacings and the edges of the partial PBG have been plotted in Fig. 4 for two different particle refractive indices.

In order to plot characteristics shown in Fig. 4, band diagrams like one shown in Fig. 3(a) were computed for PhC with fixed particle size, but different values of n and A. The computed band diagrams allowed us to extract the dependence of the PBG edges in units of A/λ versus A, and, therefore, the PBG dependence of both PBG wavelength λ and $a = A/\sqrt{2}$ was found. From these characteristics we can see that particles with $n = 2$ provide a wider PBG, but the tunability with respect to particle spacing is limited in range and has a lowest wavelength of 600 nm. However for $n = 1.6$ the PBG is narrower but has a wider tuning range with a lowest wavelength of 500 nm. For a display application the tuning range would be required to be from around 400 nm to 650 nm. Since the band diagrams are normalized to lattice constant it is straightforward to calculate the particle diameter and spacing required to cover this range. It was shown above that for $n = 1.6$ a diameter of 164 nm is required to obtain a reflection peak at 400 nm. We find that to tune this reflectivity peak to 650 nm we require a maximum lattice constant of 365 nm. The question of whether these levels of tunability in particle spacing are realizable will be discussed briefly in the conclusion and in more detail in future publications.

For display applications the absolute amount of reflectivity, not just the wavelength will be important and this cannot be obtained from the PWE method. Thus the next section uses the FDTD method to calculate the absolute reflectivity for a number of different configurations.

III. Reflection Properties of 3D PhCs Using the FDTD Method

The simulated PhC is confined within a cubic simulation domain with a side length of 2 μm as shown in Fig. 5. Simulation in a larger domain is possible, but is limited by available RAM of the computer and limitations of the computer operating system. Mur absorbing boundary conditions [15] are applied to the all sides of the simulation domain. The centres of particles in the first layer of the PhC are situated 500 nm from the bottom face of the cube, while the position of the upper layer depends on the lattice constant of the PhC.

Pulsed excitation with a spectral bandwidth covering the whole visible spectrum creates a wave propagating along z axis. Thus, one single simulation performed with the FDTD code allows us to analyze all the spectral properties of the PhC and there is no need to perform a number of simulations for excitations of different frequencies. The source of electromagnetic excitation is situated 173 nm away from the bottom face in centre of the xy plane of the simulation domain. A field probe is situated 226 nm away from the bottom edge, just in front of the source. This enables the reflection from the PhC to be calculated. The temporal dependence of field components recorded by the probes is converted into the frequency domain using Fourier transforms.

The PhC is composed of a maximum of five layers of particles and contains up to 300 single particles if $a = d$. In order to investigate this structure accurately, we have chosen to use a uniform FDTD mesh size of 13.33 nm along all directions. This cell size accurately resolves the particles themselves and is equal to $\lambda_{\mathrm{o}}/(15n)$ at the shortest wavelength considered of $\lambda_{\mathrm{o}} = 400$ nm for a refractive $n = 2$, which ensures accuracy for the FDTD method. One single simulation takes about 10 hours and requires about 650 MBytes of RAM. Since large numbers of simulations were required a Condor [17] high throughput computing cluster with more than 200 nodes was used in the work.

The pulsed TE wave injected into the simulation domain at the excitation plane is given as

$$E_y(x,y,t) = \varphi(x,y)\exp\left(-\ln(2)\sqrt{(t-\tau)/w}\right)\sin(2\pi f t) \quad (1)$$

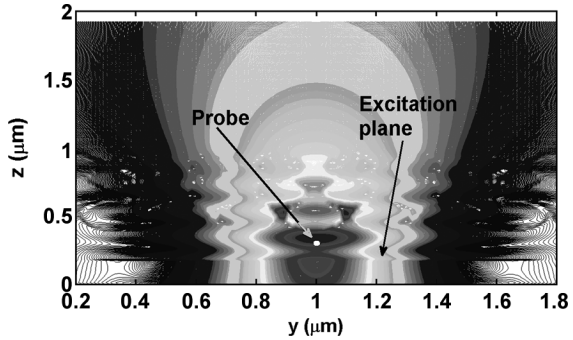

Fig. 6. Snapshot of E_y distribution across the simulation domain including the PhC made of three layers of spheres and water taken in yz plane at $x = 1\,\mu$m, $d = 200$ nm, $a = 225$ nm, $\lambda = 531$ nm. The white circle depicts the probe used to monitor the fields above the excitation.

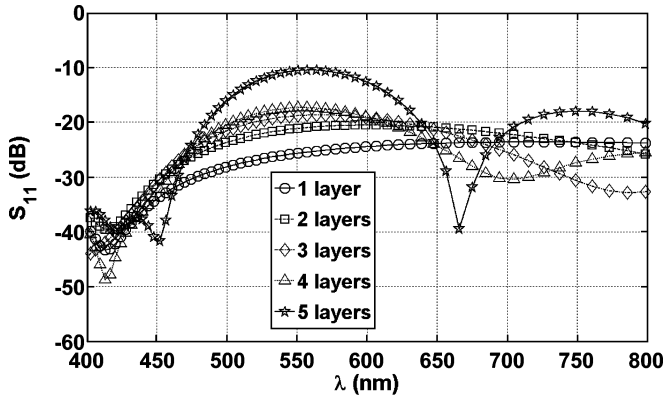

Fig. 7. Reflection coefficient spectra of the PhC with $a = 225$ nm, $d = 200$ nm and $n = 1.6$ versus the number of particle layers composing the PhC.

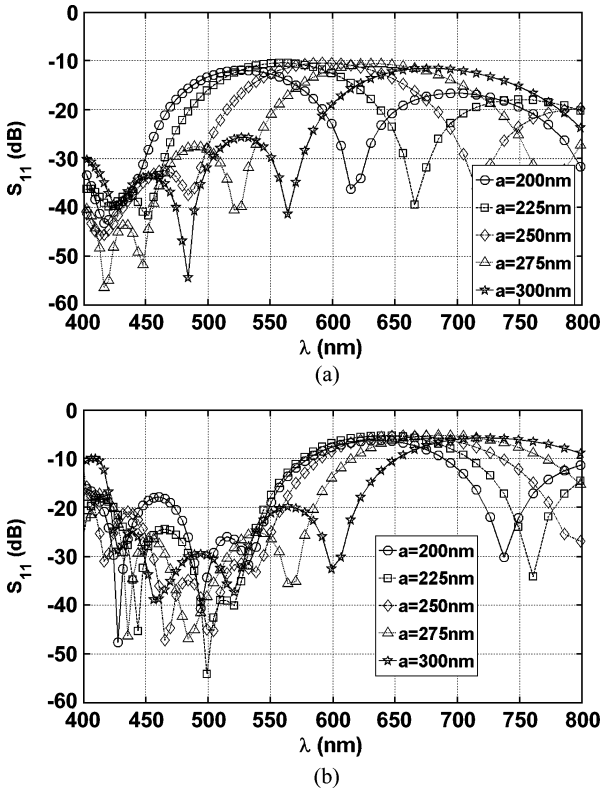

Fig. 8. Spectra of reflection coefficient versus a for refractive index of particles (a) $n = 1.6$ and (b) $n = 2$. The PhC contains five layers of particles.

where x and y are transverse coordinates, t is time, $\varphi(x, y) = \exp(-(x^2+y^2)/(2\sigma^2))$ is the transverse mode distribution, $\sigma = 500$ nm is the spatial beamwidth, $\tau = 10$ ns is the delay time, $w = 1$ ns is the pulsewidth, $f = c_0/\lambda$ is the frequency, c_0 is the vacuum speed of light and $\lambda = 531$ nm is the wavelength. This results in excitation of the structure across the whole of the visible spectrum from 400 to 800 nm.

The FDTD model provides information about transmission and reflection of waves from the PhC in both the time and frequency domains. Running Fourier transforms can be performed at particular wavelengths in order to observe the field distributions in a given plane. Fig. 6 shows the distribution of the $\mathrm{E_y}$ component at 531 nm in the y–z plane in a section through the middle of both the incident Gaussian beam and a three layer PhC. The excitation injects a TE wave with Gaussian transverse distribution of $\mathrm{E_y}$. The front of the wave becomes broader while it propagates through the PhC, but its Gaussian transverse electric field distribution survives and no diffraction is observed. In order to investigate the reflection coefficient, the time response of the fields is monitored above the excitation as shown in Fig. 6 for two cases: with and without the PhC in the simulation domain. By performing subtraction in the time domain, the reflected signal can be extracted which when Fourier transformed, gives the reflection spectra.

Fig. 7 shows the spectra of the reflection coefficient of the PhC versus number of layers of particles. The characteristics show that a reflection peak near $\lambda = 550$ nm forms when there are more than three layers; this corresponds to one period of the FCC lattice. The PhC with smaller number of layers does reflect TE waves, but its reflectivity is low and the reflection peak is spectrally wide. This behavior is as expected from simple 1D periodic structures.

The spacing between particles is then varied in order to see the band gap tuning as was observed in Section II.

Fig. 8 shows the reflection spectra versus wavelength for different particle spacing and two refractive indices $n = 1.6$ and 2.0. Both characteristics have peaks in reflection coefficient and the positions of the peaks are shown in Fig. 9. These peaks correspond to the middle of the PBGs and comparing to the PWE results shown in Fig. 4, are in agreement at large a, but less good at small a. This is due to the fact that the numerical error of both PWE and FDTD methods grows as the distance between particles approaches the size of the cell used in the method.

The results in Fig. 8 show the benefit of moving to higher refractive index in that $n = 2$ gives approximately 3 dB more reflectivity than $n = 1.6$ and in terms of displays this could be very important. The results also show that as the particles move further apart the amount of reflectivity remains reasonably constant. However at smaller particle spacing one main reflectivity peak is observed along with a residual peak at longer wavelength at approximately 6 dB lower in value. This could be in part due to the very simple way that reflectivity is being calculated in this case and a more detailed analysis under simulated daylight conditions is required before definitive statements can be made.

IV. Disorder Effects

In the previous sections perfectly ordered PhCs were considered. However, realistic PhCs exhibit particle size and position

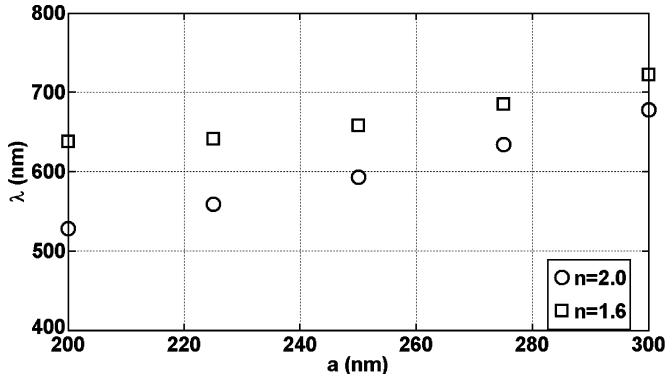

Fig. 9. Stopband of the PhC computed using FDTD method versus a.

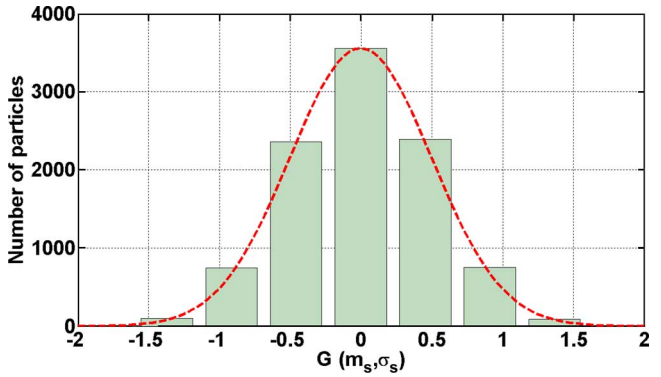

Fig. 10. Distribution of number of particles versus $G(m_s, \sigma_s)$ computed with the Gaussian random function applied in the work (bars) and the normal Gaussian distribution (dashed line) at $m_s = 0$ and $\sigma_s = 0.5$ μm. The histogram was computed for 10000 particles.

variations [4], this causes a deviation of their predicted optical properties as shown in related works [9], [10]. It is expected that a PhC created by particles in water will have variations in particle position, size and refractive index. In this work, we consider deviations of size and particle positions.

We assume that the disorder caused by the deviation of particle position is described by a Gaussian distribution [18], [19]. The distribution describes the probability of a particle occupying a position in space. The probability has a maximal value at the exact position of the particle in an ordered PhC.

Fig. 10 shows the probability density function of particles computed using the random Gaussian function [18], [19] and the normalized Gaussian distribution versus the value of $G(m_s, \sigma_s)$. As we can see, the random Gaussian function $G(m_s, \sigma_s)$ used in this work repeats the Gaussian distribution. In a randomized PhC, where the size or the position of particles may vary, most particles have diameters close to the averaged value of the diameter. Looking at Fig. 10 we can see that in this case the averaged value of the particle diameter corresponds to $G(m_s, \sigma_s) = 0$ and the probability to meet the particle of such diameter is maximal. Smaller numbers of particles have larger variation of the diameter from its average value, and this case can be modelled when $G(m_s, \sigma_s) \neq 0$. This property of the generator of random Gaussian numbers is used to approximate random disorder in the PhC.

The randomized diameter d_r of particles is then defined as

$$d_r = d + 0.25 s_s G(m_s, \sigma_s) \tag{2}$$

where d is the original non-randomized diameter of particles, s_s is the distance between particles, m_s is the mean and σ_s is the standard deviation and 0.25 is a scaling factor used to prevent overlapping between particles

The randomized x coordinate of a particle x_r is defined in a similar way as

$$x_r = x + 0.25 s_x G(m_p, \sigma_p) \tag{3}$$

where x is the non-randomized x-coordinate of the particle, s_x is the distance between particles in x direction, $G(m_p, \sigma_p)$ is the function of random Gaussian numbers, $m_p = 0$ is the mean and σ_p is the standard deviation. Randomized y_r and z_r coordinates of a particle were computed in the same way.

The polydispersity of the PhC was estimated from randomized particle diameters as $P = \overline{\sigma}_s / m_s$ [19], where $\overline{\sigma}_s = 0.25 s_s \sigma_s$ is the standard deviation for particle sizes found by fitting the particle distribution and normal Gaussian distribution as shown in Fig. 10. The standard deviation for particle x positions is defined in a similar way as $\overline{\sigma}_p = 0.25 s_x \sigma_p$. Since the mean value for particle positions is $m_p = 0$, the estimation of a quantity similar to the polydispersity using the definition from [20] is not possible. In order to analyze positional and size disorders with similar parameters in this work we normalise the positional standard deviation to the mean particle diameter, defined as $p = \overline{\sigma}_p / m_s$. The final disordered arrays of particles were produced by obtaining a random distribution and converting this to an array of particles which were then checked for overlaps. If overlaps occurred a new distribution was calculated until a non-overlapping array was obtained. The same values for σ were used in both position and diameter since both cases have the same constraint of the spacing between surfaces of adjacent particles.

Reflection coefficient spectra of the disordered PhCs were computed three times for each set of parameters of the PhC, and then averaged. Fig. 11 shows reflection coefficient spectra of the PhC versus disorder level for two values of the center-to-center spacing 225 and 300 nm. In each case two levels of polydispersity where analyzed. When $a = 225$ nm, $P = 1.56\%$ and 3.13% and when $a = 300$ nm $P = 6.25\%$ and 12.5%. This highlights the fact that as the particle spacing increases we have increasing polydispersity since the non-overlapping of particles is an important factor in the final distributions.

The figure shows that the reflection coefficient spectrum is very robust against disorder of the particle position. Fig. 12 shows the same characteristic as in Fig. 11, but for the PhC with the refractive index of particles $n = 2$. The characteristics show that the reflection spectrum of the PhC with $a = 300$ nm is slightly more sensitive to the disorder introduced than the PhC with $n = 1.6$.

Having looked at effects of particle position we now study effects of polydispersity, i.e. disorder in particle size. Fig. 13 shows the dependence of the reflection coefficient spectra versus disorder level of particle size for two values of the refractive index $n = 1.6$ and $n = 2$. These dependencies show that the PhC with the smaller refractive index of particle has only one narrow peak at lower wavelengths and the disorder does not introduce any more intense reflection peaks. Therefore, the PhC with smaller refractive index of particles must be more attractive

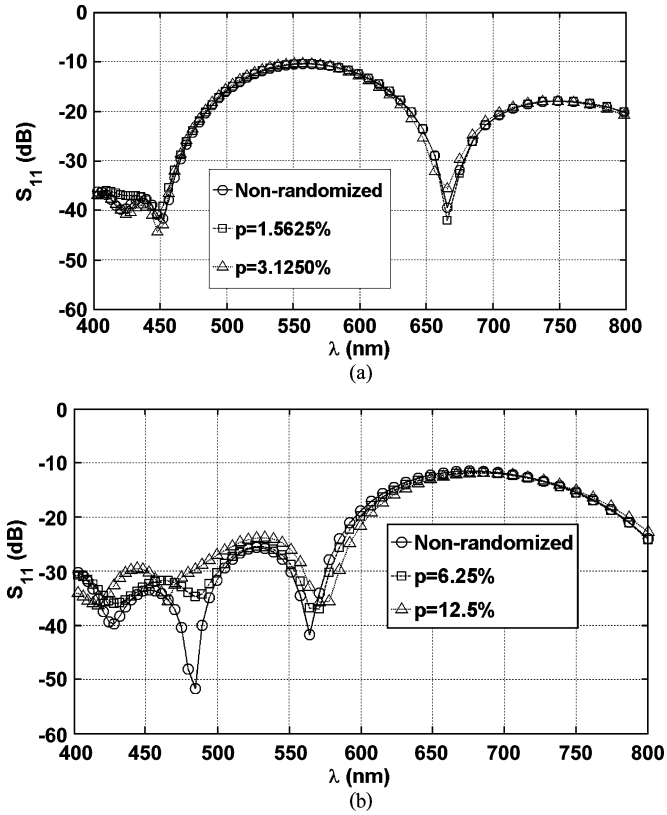

Fig. 11. Reflection coefficient spectra versus disorder level of particle position given by the standard deviation σ_p for the PhC with the centre-to-centre spacing $a = 225$ nm (a) and $a = 300$ nm (b). The refractive index of particles $n = 1.6$.

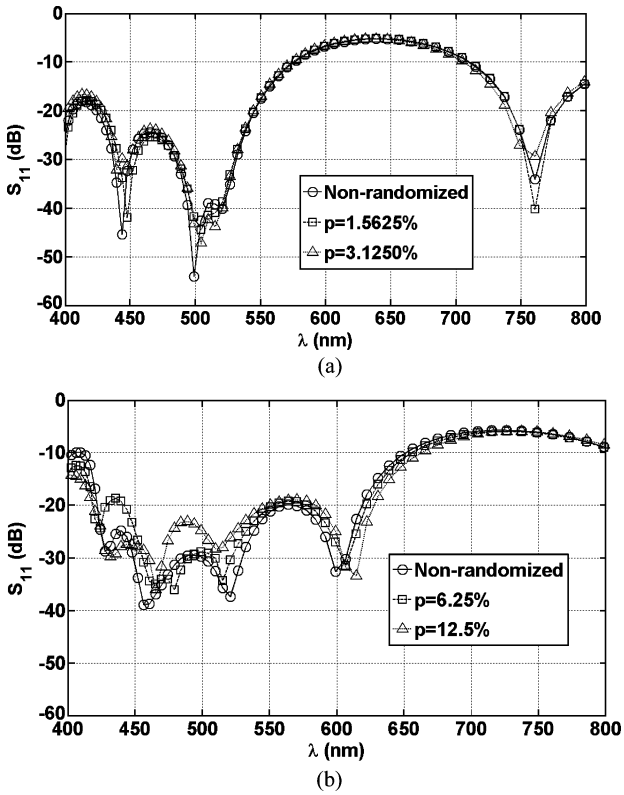

Fig. 12. Reflection coefficient spectra versus disorder level of particle position given by the standard deviation σ_p for the PhC with the lattice constant $a = 225$ nm (a) and $a = 300$ nm (b) the refractive index of particles $n = 2$.

for the display applications because their reflection spectrum is less sensitive to the variations in particle diameters of the PhC.

V. Discussion

The above sections have shown encouraging results for display applications, however there are some important parameters for displays that can be further investigated. Thus this section will discuss reflectivity, color gamut and contrast ratio with reference to other display technologies and will show preliminary results for viewing angle sensitivity.

In terms of reflectivity, the maximum value shown here is for five layers of $n = 2$ particles and is around -7 dB or in terms of reflectance 20%. By adding another 5 layers this could be increased to 40%. This compares to 40% for electrophoretic displays (E-ink), 30% for cholesteric liquid crystal (Kent Displays Inc.), >50% for electrowetting (Liquavista), up to 65% for electrochromic (DIC), 25% for micro-electromechanical interference (Qualcomm Inc.) and 40% for liquid powder (Bridgestone) [24]. With a further increase in the number of PhC layers to around 20 this display could even approach that of ink on white paper which gives a reflectance of 80% [24]. Another advantage of the direct color reflection approach is that no color filter layers are required. This is because the filters are generally pigment based absorbers and their transmittance 'T' is related to their absorbance 'α' and thickness 'd' by $T = \exp(-2\alpha \mathrm{d})$ so that in order to get the same optical performance as a transmissive display, either the thickness of the layer or the absorbance has to be halved in a reflective display. This leads to poor color saturation, and color purity.

The color gamut and color coordinates are dependent upon the quality of the three primaries used to create the display. Since this is PhC based device, the primaries can in principle be very narrow and pure. This display also has the added benefit that the reflectance peak can be tuned to any wavelength in order to improve the gamut.

The contrast ratio will be the difference in reflectance between the ordered and the completely disordered state where no voltage is applied. Typical values achieved by other emerging display technologies are 8.5:1 for E-Ink [25] and up to 450:1 in a dye-doped reflective LC display [26]. Reflective cholesterics generally have a contrast ratio around 10:1, in-plane electrophoretic devices can also get contrast ratios of up to 11.3:1 [27] The achievable contrast for the display shown here, has been investigated using the 3D FDTD model. We have taken a typical case shown for five layers of 200 nm, $\mathrm{n} = 1.6$ particles at a spacing of 225 nm as shown in Fig. 7. We have then allowed the 225 particles which made up the ordered PhC to be placed randomly, with no overlaps between particles in order to simulate the case with no voltage applied. Fig. 14 shows a comparison between these two cases and it can be seen that a contrast of $\sim$10 dB (10:1) is obtained. It is felt that with more layers in the ordered PhC in combination with a dark background to the pixel much higher contrasts could be achieved.

Finally, we have attempted to quantify the angular sensitivity of the reflectivity. We have done this by rotating the structure in the simulation domain and measuring the reflected signal at

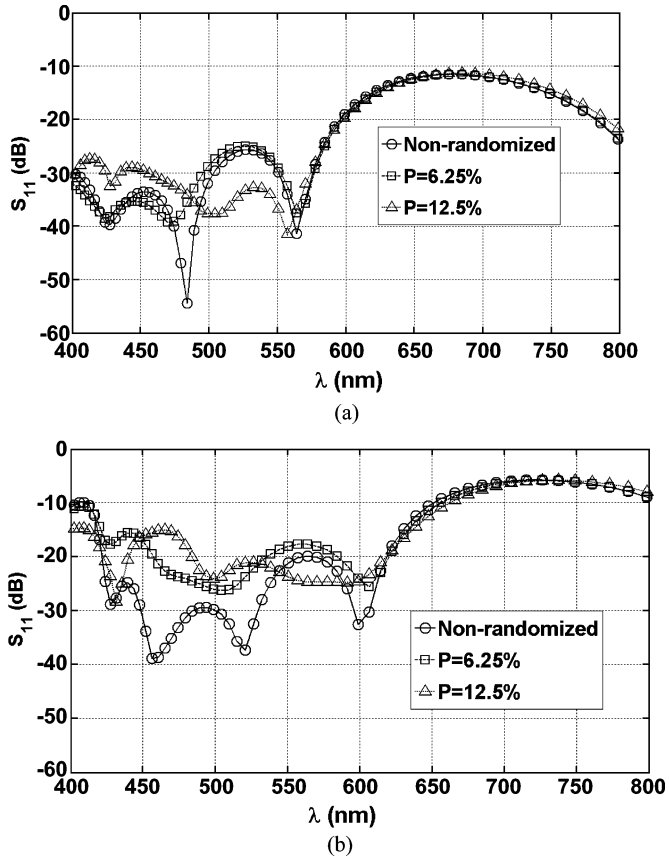

Fig. 13. Reflection coefficient spectra versus disorder level of particle size given by the standard deviation σ_s for the PhC with the lattice constant $a = 300$ nm (a). The refractive index of particles $n = 1.6$ and (b) $n = 2$.

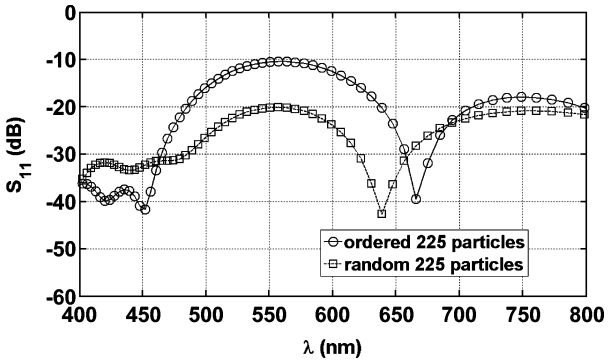

Fig. 14. Reflection coefficient spectra of the ordered PhC consisting 5 layers of particles with the lattice constant of $a = 225$ nm, the particle diameter is $d = 200$ nm and a the disordered case with random particle positions chosen according to uniform distribution of random numbers. The refractive index of particles is $n = 1.6$.

what would have been normal reflection in the un-rotated structure. Ideally we would want to measure the direct specular reflection, but this non-specular reflectivity gives a good indication to the sensitivity. The results are shown in Figs. 15 and 16 for two different particle spacings up to an angle of 12 degrees off normal (24 degrees total angle due to symmetry). Fig. 15 shows a very small variation in reflection, while Fig. 16 shows a slightly higher variation at around 2–3 dB at peak reflection. Remembering that this is non-specular reflection it is hoped that with larger numbers of layers operating in full daylight angular

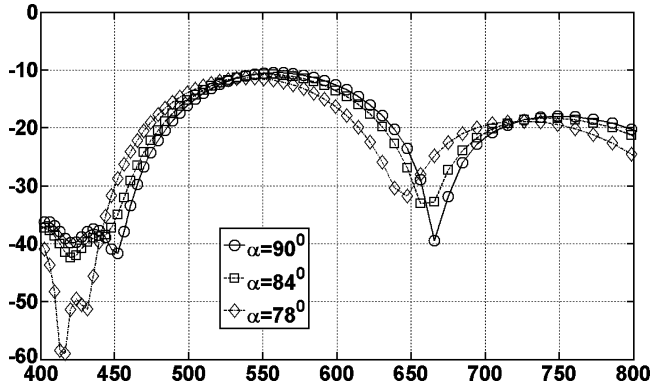

Fig. 15. PhC reflection coefficient spectra versus the inclination angle of PhC consisting 5 layers of particles. $\alpha = 90$ deg corresponds to normal incidence on the PhC. The PhC lattice constant of $a = 225$ nm, the particle diameter is $d = 200$ nm, the refractive index of particles is $n = 1.6$.

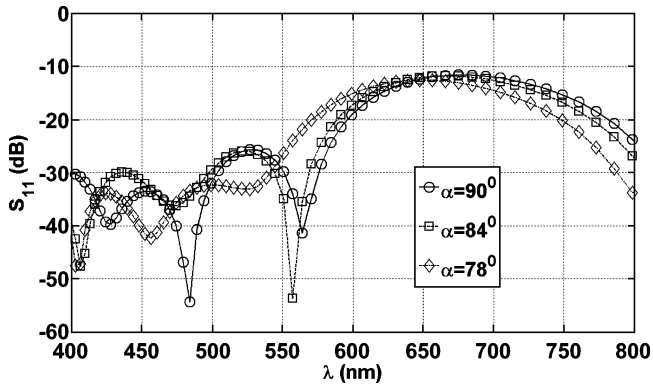

Fig. 16. Reflection coefficient spectra versus the inclination angle of PhCs consisting 5 layers of particles. The PhC lattice constant is $a = 300$ nm, the particle diameter is $d = 200$ nm, the refractive index of particles is $n = 1.6$. $\alpha = 90$ deg corresponds to normal incidence on the PhC.

sensitivity could be reduced to an acceptable level. It should also be pointed out that there are known methods to broaden viewing angle such as using scattering films on the top surface of the display [28].

VI. Conclusion

This paper has used full 3D modeling to study the performance of a tunable 3D photonic crystal system which has potential application in next generation reflective display technology. The paper predicts that 164-nm diameter latex particles with refractive index of 1.6 could provide stop band tuning across the visible spectrum. Further work is needed to understand whether the required lattice constant tuning is experimentally achievable with this system, and it may be that other host-particle combinations are required such as non-aqueous solutions to achieve this. The paper then addresses the issue that in real systems, some randomization of the particle positions will occur, and the particle size will not be completely uniform, showing some degree of polydispersity. Using random distributions, bounded by the particle spacing, the effect of positional disorder is studied. The results show that disorder has very little effect on the main $\Gamma - \mathrm{L}$ stopband. The effects of polydispersity are then investigated and this system again shows robust reflection peaks in this case. Finally a discussion on more realistic display parameters such as

contrast ratio, color gamut and reflectivity is undertaken along with further modeling results. The potential performance of this technology is also compared with other competing approaches and some preliminary results for viewing angle sensitivity are shown. The study of reflectivity in this work is based on a simple single point probing of the reflected fields and future work will move towards a more realistic model of daylight illumination.

REFERENCES

[1] T. A. Birks, J. C. Knight, and P. S. J. Russell, "Endlessly single-mode photonic crystal fiber," *Opt. Lett.*, vol. 22, pp. 961–963, 1997.

[2] H. J. Unold, S. W. Machmoud, R. Jaeger, M. Golling, M. Kicherer, F. Mederer, M. C. Riedl, T. Knoedl, M. Miller, R. Michalzik, and K. J. Ebeling, "Single-mode VCSELs," in *Proc. SPIE*, 2002, vol. 4649, pp. 218–229.

[3] A. C. Arsenault, T. J. Clark, G. von Freymann, L. Cademartiri, R. Sapienza, J. Bertolotti, E. Vekris, S. Wong, V. Kitaev, I. Manners, R. Z. Wang, S. John, D. Wiersma, and G. A. Ozin, "From colour fingerprinting to the control of photoluminescence in elastic photonic crystals," *Nature Mater.*, vol. 5, pp. 179–184, 2006.

[4] D. R. E. Snoswell, C. L. Bower, P. Ivanov, M. J. Cryan, J. G. Rarity, and B. Vincent, "Dynamic control of lattice spacing within colloidal crystals," *New J. Phys.*, vol. 8, p. 267, 2006.

[5] W. Wohlleben, S. Altmann, F. Bartels, S. Fischer, and R. J. Leyrer, "Tunable, elastic, crack-free photonic crystals and polymer opal templates with pre-determined orientation for defect inscription," in *Proc. CLEO-IQEC Eur. 2007*, 2007, p. 1, VDE Verlag GMBH.

[6] "Control of lattice spacing within photonic crystals," Patent WO/2009/060166, May 14, 2009.

[7] D. R. E. Snoswell, R. K. Brill, and B. Vincent, "pH-Responsive microrods produced by electric-field-induced aggregation of colloidal particles," *Adv. Mater.*, vol. 20, pp. 1–4, 2008.

[8] A. C. Arsenault, D. P. Puzzo, I. Manners, and G. A. Ozin, "Photonic crystal full colour displays," *Nature Photon.*, vol. 1, p. 468, 2007.

[9] A. Rodriguez, M. Ibanescu, J. D. Joannopoulos, and S. G. Johnson, "Disorder-immune confinement of light in photonic-crystal cavities," *Opt. Lett.*, vol. 30, pp. 3192–3194, 2005.

[10] A. V. Lavrinenko, W. Wohlleben, and R. J. Leyer, "Effect of disorder on transmission characteristics of finite inverse-opal photonic crystals," in *Proc. Symp. on Photonic and Electromagn. Crystal Structures*, 2007.

[11] M. Allard and E. H. Sargent, "Impact of polydispersity on light propagation in colloidal photonic crystals," *Appl. Phys. Lett.*, vol. 85, pp. 5887–5889, 2004.

[12] C. J. Railton and G. S. Hilton, "The analysis of medium sized arrays of complex elements using a combination of FDTD and reaction matching," *IEEE Trans. Antenna Propagat.*, vol. 47, no. 4, pp. 707–714, Apr. 1999.

[13] RSOFT Design Group, "RSOFT Software," [Online]. Available: www.rsoftdesign.com

[14] A. Yethiraj and A. van Blaaderen, "A colloidal model system with an interaction tunable from hard sphere to soft and dipolar," *Nature*, vol. 421, p. 513, 2003.

[15] M. C. Concalves, J. Bras, and R. M. Almeida, "Process optimization of sol-gel derived colloidal photonic crystals," *J. Sol.-Gel. Sci. Technol.*, vol. 42, pp. 135–143, 2007.

[16] G. Mur, "Absorbing boundary conditions for the finite-difference approximation of time-domain electromagnetic field equations," *IEEE Trans. Electromagn. Compat.*, vol. EMC-23, no. 4, pp. 377–382, Nov. 1981.

[17] Condor Team, Computer Sciences Dep., Univ. Wisconsin—Madison, "Condor software," [Online]. Available: http://www.cs.wisc.edu/condor/

[18] D. B. Thomas, W. Luk, P. H. W. Leomg, and J. D. Villasenor, "Gaussian random number generators," *ACM Comput. Surveys*, vol. 39, p. 11, 2007.

[19] Calif. Inst. of Technol., Pasadena, "Math à la carte, Gaussian (normal) random numbers and vectors," 2008 [Online]. Available: http://www.mathalacarte.com/

[20] D. A. Kofke and P. G. Bolhuis, "Freezing of polydisperse hard spheres," *Phys. Rev. E*, vol. 59, pp. 618–622, 1999.

[21] R. M. Amos, J. G. Rarity, P. R. Tapster, T. J. Shepherd, and S. C. Kitson, "The fabrication of large area FCC hard sphere colloidal crystals by shear alignment," *Phys Rev E*, vol. 61, p. 2929, 2000.

[22] M. M. Sigalas, C. M. Soukoulis, C. T. Chan, R. Biswas, and K. M. Ho, "Effect of disorder on photonic band gaps," *Phys. Rev. B*, vol. 59, pp. 12767–12770, 1999.

[23] Z.-Y. Li and Z.-Q. Zhang, "Fragility of photonic band gaps in inverse-opal photonic crystals," *Phys. Rev. B*, vol. 62, pp. 1516–1519, 2000.

[24] J. Heikenfeld, K. Zhou, E. Kreit, B. Raj, S. Yang, B. Sun, A. Milarcik, L. Clapp, and R. Schwartz, "Electrofluidic displays using Young-Laplace transposition of brilliant pigment dispersions," *Nature Photon.*, vol. 3, pp. 292–296, May 2009.

[25] Y. Chen, J. Au, P. Kazlas, A. Ritenour, H. Gates, and J. Goodman, "Ultra-thin, high-resolution, flexible electronic ink displays addressed by a-Si active-matrix TFT backplanes on stainless steel foil," in *IEEE Electron Devices Meeting (IEDM '02)*, 2002, pp. 389–392.

[26] Y.-H. Lin, J.-M. Yang, Y.-R. Lin, S.-C. Jeng, and C.-C. Liao, "A polarizer-free flexible and reflective electrooptical switch using dye-doped liquid crystal gels," *Opt. Expr. 1777*, vol. 16, no. 3, Feb. 2008.

[27] E. Kisha, Y. Matsuda, Y. Uno, A. Ogawa, T. Goden, N. Ukigaya, M. Nakanishi, T. Ikeda, H. Matsuda, and K. Eguchi, "Development of in-plane EPD," in *SID Tech. Dig.*, 2000, vol. 31, p. 24.

[28] T. Uchida, T. Nakayama, T. Miyashita, M. Suzuki, and T. Ishinabe, "A novel reflective liquid crystal display with high resolution and full color capability," *Jpn. J. Appl. Phys.*, vol. 43, pp. 8094–8100, 2004.

Pavel Ivanov, photograph and biography not available at time of publication.

Y.-L. D. Ho, photograph and biography not available at time of publication.

David R. E. Snoswell, photograph and biography not available at time of publication.

Nils Elsner, photograph and biography not available at time of publication.

Brian Vincent, photograph and biography not available at time of publication.

Chris Bower, photograph and biography not available at time of publication.

John G. Rarity, photograph and biography not available at time of publication.

Martin J. Cryan, photograph and biography not available at time of publication.